

Synthesis Processing Condition Optimization of Citrate Stabilized Superparamagnetic Iron Oxide Nanoparticles using Direct Co-Precipitation Method

Mubarika Sekarsari Yusuf, Sutriyo* and Ratika Rahmasari

Faculty of Pharmacy, Universitas Indonesia, Depok, Indonesia.

*Corresponding Author E-mail: sutriyo@farmasi.ui.ac.id

<https://dx.doi.org/10.13005/bpj/2255>

(Received: 19 August 2021; accepted: 24 September 2021)

Superparamagnetic iron oxide nanoparticles (SPION) are commonly prepared by co-precipitation, a convenient and high yield producing method. However, this method produces large particles and wide size distribution. Thus, this study aims to optimize and determine the processing condition during the direct co-precipitation synthesis of citrate stabilized SPION (SPION-C). Processing conditions were optimized to achieve the suitable hydrodynamic size and zeta potential; measured straight after preparation, at weeks 3, 10, and 30. Characterization of optimized SPION and SPION-C was done by Fourier transform infrared spectroscopy (FTIR), fluorescence spectroscopy, X-ray diffraction (XRD), and transmission electron microscopy (TEM). The optimized processing condition (stirring speed of 9000 rpm, stabilizer concentration of 1.006 M, and a 90°C stabilizer adsorption temperature), resulted in suitable SPION-C with a hydrodynamic size of 25.94 ± 2 nm, and zeta potential value of -50.8 ± 3.9 . Particles with an almost sphere morphology with below 20 nm size were shown by TEM. The XRD analysis presented magnetite phase with a 2.79 nm core size which indicated the formation of stabilized SPION. The maximum excitation and emission wavelength of SPION after stabilization were proved to be uninterrupted by fluorescence spectroscopy. Further FTIR results supported the successful conjugation of citrate onto SPION. Highly stable and crystalline SPION-C were successfully produced through an optimized processing condition using direct co-precipitation. The obtained SPION-C conveyed desired nanoparticle size with narrow size distribution and stability for 30 weeks of storage at 4°C.

Keywords: Citrate; Direct Co-Precipitation; Processing Conditions
Superparamagnetic Iron Oxide Nanoparticles.

Metallic nanoparticles (MNP) have been proved useful in the biomedical field and have been studied vastly in recent years, specifically superparamagnetic iron oxide nanoparticles (SPION). These MNP diagnostic agents are useful for magnetic resonance imaging (MRI) ¹⁻³. Diagnostic agents in delivery systems will aid to confirm the precise and successful biodistribution of therapeutic agents ⁴. This unique MNP only

shows magnetization properties under the influence of a magnetic field⁵, making them instantly detectable through MRI to trace drug distribution in the human body⁶. Moreover, they can also become an important component in drug delivery and targeting systems and nevertheless hyperthermia therapy^{3,4,7,8}.

Despite being biocompatible, the biomedical effectiveness of SPION heavily

depends on their physical stability. Since SPION are lyophobic, in an aqueous environment, they tend to aggregate to one another. Thermodynamically, these nanoparticles are more stable to interact with one another than with water because of their incapability to form hydrogen bonds⁹⁻¹¹. Ensuring the physical stability of synthesized SPION is crucial to prevent the growth of its particle size and platelet aggregation after administration.

Stabilization of SPION has previously been accomplished with molecules including trisodium citrate dihydrate, oleic acid, and polymers. These molecules decrease and prevent particle growth and guarantee its physical stability. Advantages of trisodium citrate dihydrate as a stabilizer include affordable, abundant, and can create high dispersible SPION in aqueous solvents.

The direct co-precipitation method for superparamagnetic iron oxide nanoparticle synthesis is known to be convenient, uses lower temperatures, nonetheless produces high yields. Meanwhile, this cost-effective method isn't free from drawbacks; mainly high polydispersity and large particle size. For superparamagnetic properties, core size of below 20 nm would have to be reached, though different works of literature have also stated 30 – 50 nm¹², or <150 nm for magnetic particle imaging¹³. Besides achieving the desired nanoparticle size, the surface coating can also prevent oxidation of SPION from the environment¹⁴.

To overcome the limitations of the direct co-precipitation method, this research focuses on optimizing the processing conditions including stirring speed, stabilizer concentration, and stabilizer adsorption temperature. The stability of SPION will be measured by hydrodynamic size, polydispersity index, and zeta potential. Furthermore, physicochemical characteristics from the most preferable processing condition will be observed by FTIR, fluorescence spectroscopy, XRD, and TEM. The stable SPION-C produced is expected to be used directly or conjugated onto another molecule.

MATERIALS AND METHODS

Reagents and instruments

Iron (III) chloride hexahydrate ($\text{FeCl}_3 \cdot 6\text{H}_2\text{O}$), iron (II) chloride tetrahydrate ($\text{FeCl}_2 \cdot$

$4\text{H}_2\text{O}$), ammonia solution (25%), and trisodium citrate dihydrate, were from Merck, Germany. Nanoparticles were analyzed by a NANO-ZS series Malvern Zetasizer (Malvern Instruments, Malvern, UK) particle size analyzer, and a Hitachi HT-7700 transmittance electron microscope (TEM), Institut Teknologi Bandung. Crystalline characteristics were observed using an X-ray diffractometer (PANalytical X'Pert), whilst other physicochemical properties were observed using an FTIR spectrophotometer 8400 S (Shimadzu, Japan); and Horiba FluoroMax Hybrid Fluorescence Spectroscopy Steady State and Life Time System (Integrated Laboratory & Research Center Universitas Indonesia).

Synthesis of citrate stabilized superparamagnetic iron oxide nanoparticles

Citrate stabilized superparamagnetic iron oxide nanoparticles were synthesized using the direct co-precipitation method based on previous literature^{15,16} with some modifications. FeCl_3 solution (50 mL, 0.08 M) and FeCl_2 solution (50 mL, 0.04 M) were prepared separately in demineralized water. The prepared solution of FeCl_3 was poured carefully into the three-neck round bottom flask, followed by the solution of FeCl_2 under a nitrogen atmosphere. Both solutions were mixed under vigorous stirring (3000 – 12000 rpm) using an IKA EUROSTAR 20 high-speed digital overhead stirrer. The volume of the mixture was then added to 150 mL with continued stirring and its temperature was increased to 60°C before adding the ammonia solution dropwise until the solution reached above pH 9. Instantly, the solution turned dark brown to black and the reaction was held for 15 minutes at a constant temperature. Trisodium citrate dihydrate solution (10 mL, 0.503 M or 10 mL, 1.006 M) was added to the reaction after the product reached 90°C and left for an hour while maintaining stable temperature and stirring speed. Molar ratio of $\text{FeCl}_3 \cdot 6\text{H}_2\text{O}$ to $\text{FeCl}_2 \cdot 4\text{H}_2\text{O}$ of all batches was 2:1. Once the optimal speed and stabilizer concentration was determined, the temperature for stabilizer adsorption was studied.

Particle size, PDI, and zeta potential measurement

Hydrodynamic particle size, polydispersity index (PDI), and zeta (ζ) potential of SPION and SPION-C were analyzed by dynamic light scattering (DLS) at room temperature. The sample

solution was prepared with a concentration of 5 $\mu\text{L}/\text{mL}$ in water.

FTIR analysis

Chemical functional groups present on the synthesized SPION and SPION-C were analyzed and confirmed by infrared spectroscopy with transmittance (%) measured at a 4000 – 400 cm^{-1} .

Fluorescence spectroscopy

The excitation and emission spectrum of SPION and SPION-C were determined by fluorescence spectroscopy.

XRD analysis

Crystalline characteristics of SPION and SPION-C were observed by X-ray diffraction (XRD), using a Copper K- α ($\lambda = 1.5 \text{ \AA}$) radiation source with generator settings of 30 mA and 40 kV, and a 0.02° step size; Bragg angle from 10° to 90°. Rietveld refinement was done using the PANalytical X'Pert HighScore Plus program.

Morphological analysis

Individual SPION-C and their core size along with their morphological shape were analyzed by TEM where a drop of diluted SPION-C was placed on a 20 nm Cu: Carbon TEM mesh grid and let dry before analysis.

Stability during storage

The stability study of SPION-C at 4°C was to resemble the storage condition of the nanoparticles. Particle size, PDI, and zeta potential were observed for up to 30 weeks.

RESULTS AND DISCUSSION

SPION stabilized by trisodium citrate dihydrate has successfully been synthesized through direct co-precipitation by optimizing their processing conditions (Table 1).

Influence of stirring speed

The mean of size distribution by number of SPION-C from smallest to largest was Batch E, C, B, and F (Table. 2). Batches C (6000 rpm) and E (9000 rpm) obtained smaller hydrodynamic sizes than previous studies of citrate stabilized SPION synthesized by co-precipitation which were larger than 200 nm¹⁷, 100 nm¹⁸, and 55 nm¹⁹.

As the hydrodynamic sizes of SPION of batch A and batch D were similar (Table. 2), our study demonstrates that stirring speed greatly influences the success of stabilizer adsorption and eventually the SPION-C end particle size. Stirring speed effects, the reaction environment of SPION-C during the addition and adsorption of citrate ions onto SPION. Hence, the surface modification of the nanoparticles by the addition of a stabilizer drastically suppresses the nanoparticle size²⁰.

Superparamagnetic iron oxide nanoparticle synthesis starts with the core formation, followed by nucleus growth. The latter needs to be prevented at the correct designate to achieve the intended

Table 1. Processing conditions of SPION and SPION-C

Batch	Stirring speed (rpm)	Stabilizer concentration	Stabilizer adsorption
A	3000	-	-
B	3000	0.503 M	90°C
C	6000	0.503 M	90°C
D	9000	-	-
E	9000	0.503 M	90°C
F	12000	0.503 M	90°C
G	9000	1.006 M	90°C
H	9000	1.006 M	60°C

Table 2. Influence of stirring speed on SPION and SPION-C

Batch	Stirring speed (rpm)	Stabilizer concentration	Size ^I \pm SD ^{II} (nm)	PDI \pm SD ^{II}	ζ potential \pm SD ^{II} (mV)
A	3000	-	1357.07 \pm 583	-	-24.3 \pm 1.1
B	3000	10 mL, 0.503 M	39.95 \pm 16	0.243 \pm 0.02	-48.63 \pm 3.0
C	6000	10 mL, 0.503 M	36.56 \pm 8	0.339 \pm 0.05	-37.1 \pm 6.5
D	9000	-	854.97 \pm 169	-	-30.8 \pm 0.6
E	9000	10 mL, 0.503 M	25.58 \pm 7	0.346 \pm 0.01	-41.67 \pm 2.1
F	12000	10 mL, 0.503 M	161.27 \pm 33	-	-38.17 \pm 1.8

^ISize distribution by number

^{II}SD standard deviation (n=3)

size for nanoparticles to obtain superparamagnetic properties. Nuclei or crystal growth is inhibited by the adsorption of citrate ions on the surface of SPION which stabilizes and prevents these particles from aggregation²⁰. Amid this step, the rate of inhibition by the stabilizer will influence the resulting hydrodynamic size of the nanoparticles. After the black precipitate formation at basic conditions, the stabilizer solution should be rapidly distributed throughout the SPION solution.

An increase of stirring speed from 3000 rpm to 9000 rpm improved nanoparticle hydrodynamic size from thousands of nanometers to below 30 nm, as shown by batch B and E (Table 2). Essentially, the purpose of stirring is to create a homogenous solution. Stirring speed influences fluid flow, where within the fluids are the residing nanoparticles, and therefore different stirring speeds will cause the SPION and TCD to migrate and interact with each other at different rates²¹. Nonetheless, in our case, at very high speeds (12000 rpm), parameters of SPION-C were found

to be less preferable. Agglomeration leading to higher hydrodynamic size initiated by the immense interaction of particles is believed to be the reason. Smaller SPION-C might also have aggregated, forming larger clusters leading to an increase in hydrodynamic size and poor polydispersity due to various cluster sizes²², but similar ζ potential for all SPION-C batches. Our findings show that different stirring speeds influence the hydrodynamic size of the SPION-C, and at very high speeds, their polydispersity indexes.

All SPION showed negative ζ potential ranging from 23.23 mV to 31.3 mV, and ζ potential of SPION-C for batches B, C, E, and F ranged from -30.6 mV to -52.0 mV ($B > E > F > C$) as seen in Table. 2, meaning that all SPION-C have moderate (31 – 40 mV) to fairly good (41 – 60 mV) colloidal stability²³. The increase in ζ potential of SPION after stabilization was up to 28.8 mV, surpassing previous literature^{10,25}. Without stabilization, SPION acquired less stability shown by their lower ζ potential. Visually, SPION would sediment

Table 3. Influence of stabilizer concentration on SPION-C

Batch	Stirring speed (rpm)	Stabilizer concentration	Size ^I \pm SD ^{II} (nm)	PDI \pm SD ^{II}	ζ potential \pm SD ^{II} (mV)
E	9000	0.503 M	25.58 \pm 7	0.346 \pm 0.01	-41.67 \pm 2.1
G	9000	1.006 M	25.94 \pm 2	0.312 \pm 0.09	-50.8 \pm 3.9

^ISize distribution by number

^{II}SD standard deviation (n=3)

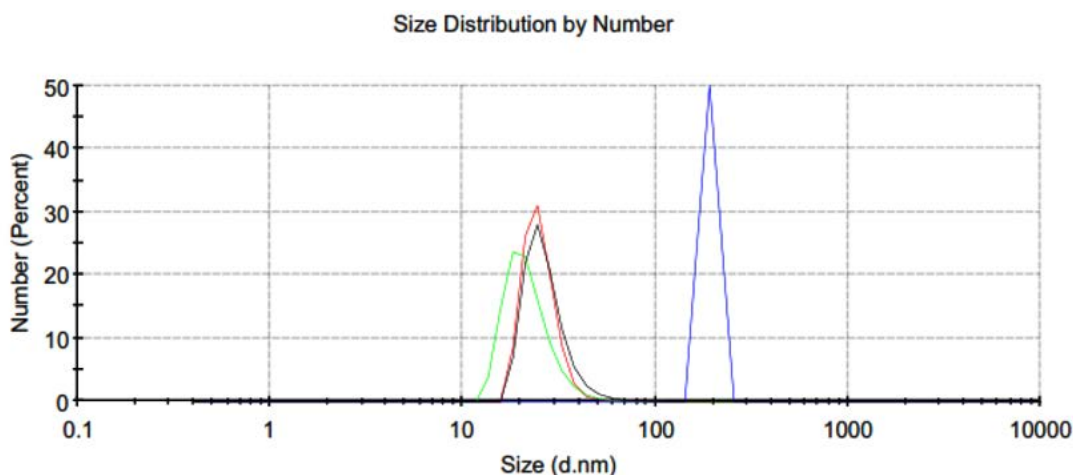


Fig. 1. Effect of stirring speed on the particle size of SPION-C (Red) Batch B/3000 rpm; (Black) Batch C/6000 rpm; (Green) Batch E/9000 rpm (Blue) Batch F/12000 rpm

substantially faster than SPION-C for all process conditions. After approximately 15 minutes¹², a clear borderline between the sediment (SPION) and the solvent can be distinguished, whereas the SPION-C still presented a black homogenous solution (Table 4).

Citrate possesses three carboxylate functional groups where at least one will face outwards on the SPION-C's surface upon adsorption which accounts for their negative and higher ζ potential compared to SPION^{23,24}. The citrate ions create steric hindrance to prevent SPION from interacting with each other¹². Such steric hindrance is categorized as electro kinetic stabilization originating from anionic carboxyl groups. Besides fabrication of hydrophilic SPION, the free carboxyl group facing out to the solvent will aid SPION to be

conjugated or functionalized to another molecule, for example, a drug, carrier, or fluorescent dye.




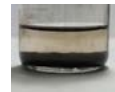








Influence of stabilizer concentration

Comparing batch E to G, twice as much stabilizer concentration resulted in a narrower polydispersity index (0.346 to 0.312) and better stability (-41.7 mV to -50.8 mV) of SPION-C. The availability of the stabilizer was more precise as it had better coverage on the surface of the SPION. Moreover, as its concentration was higher, the time for it to be distributed in the solution was fast enough to prevent larger nanoparticle growth.

Influence of stabilizer adsorption temperature

Two different temperatures for citrate adsorption experimented were at 60°C and 90°C. It was shown that the temperature affects the reaction temperature during stabilizer addition and highly

Table 4. Influence of stabilizer adsorption temperature on SPION-C

Variation	Size ^I ± SD ^{II} (nm)	ζ potential ± SD ^{II} (mV)	Initial	Sedimentation time		
			1 hour	2 hours	3 hours	
SPION, no citrate adsorption (Batch D)	854.97 ± 169	-30.8 ± 0.6				
SPION-C, adsorption at 60°C (Batch H)	278.33 ± 109	-43.2 ± 1.7				
SPION-C, adsorption at 90°C (Batch G)	25.94 ± 2	-50.8 ± 3.9				

^ISize distribution by number

^{II}SD standard deviation (n=3)

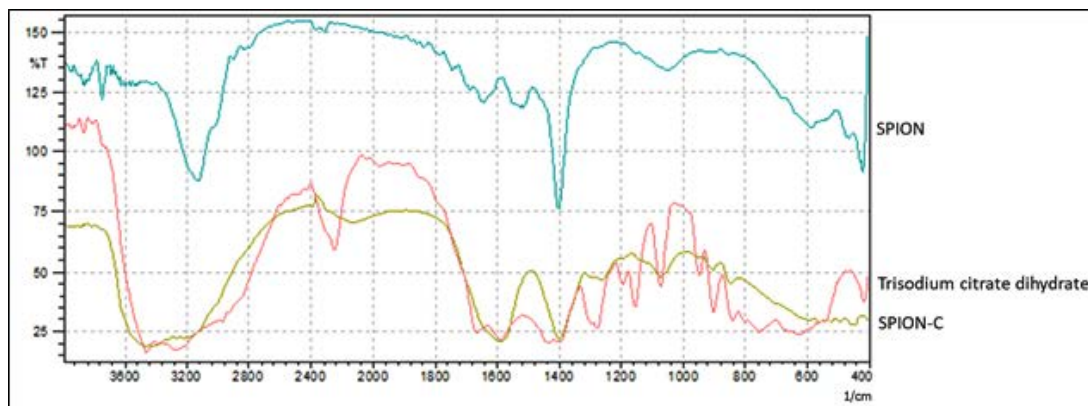


Fig. 2. FTIR spectrum of SPION, trisodium citrate dihydrate, and SPION-C

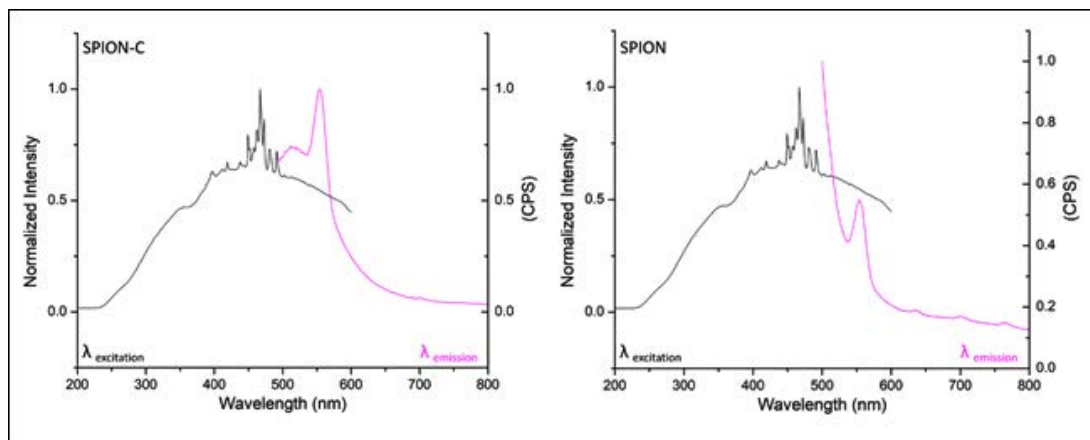


Fig. 3. Fluorescence spectroscopy of SPION and SPION-C

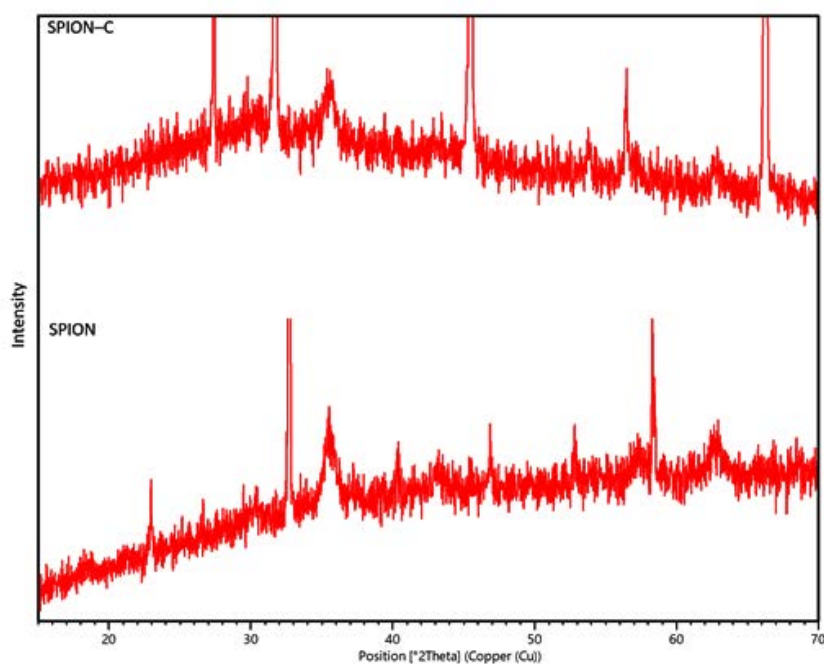


Fig. 4. XRD intensity peaks of SPION and SPION-C

determines the success of citrate adsorption onto the SPION surface (Table 4.) Over the SPION growth phase, an elevated temperature is required to aid citrate adsorption onto the nanoparticles' surface, as higher temperatures accelerate the chemical adsorption process²². SPION-C produced with the lower temperature sedimented at a higher velocity. This can be explained by failure the of the citrates' carboxyl groups to be adsorbed completely

onto the SPION surface. Therefore, on its surface areas where citrate isn't available, SPION can interact with each other, meaning less stabilization and leading to particle growth¹². After 3 hours there was a clear difference between batch D, G, H, and being the most stable, was batch G. Visual results are also reinforced by the particle size and ζ potential where the partially stabilized SPION (batch H) have a larger particle size and lower

æ potential than fully stabilized SPION (batch G), however a smaller particle size and higher æ potential than SPION (batch D).

FTIR analysis

The fingerprint of iron oxide (Fe-O) from SPION is noticeable at 584.45 cm^{-1} (Fig. 1) where stated in previous literature corresponds to magnetite. The appearance of new bands at 1200 cm^{-1} , 900 cm^{-1} , and 850 cm^{-1} on SPION-C proves the presence of citrate on the nanoparticles. The chemical bond is believed to happen between carboxyl groups from trisodium citrate dihydrate and hydroxyls of iron oxides through esterification^{12,26}.

Strong broad bands stretching from $3500 - 2500\text{ cm}^{-1}$ correspond to the vibrational stretching of -CH and -OH of carboxylate functional groups of SPION-C which are also found on the trisodium citrate dihydrate (TCD) spectrum but have slightly shifted to a higher wavelength. The vibrational asymmetric stretching of SPION-C at 1589.40 cm^{-1} assigns to carbonyl (C=O), and at 1200 cm^{-1}

points the C-O single bond of the adsorbed citrates. Crowded peaks between $1600 - 1200$ of TCD have shifted after TCD conjugation to SPION as seen in SPION-C²⁷. Analyzing the FTIR spectrum confirms that citrate has been successfully coated onto the surface of SPION.

Fluorescence spectroscopy

Both SPION and SPION-C had excitation maximum at $\lambda 467\text{ nm}$ and emission maximum at $\lambda 554 - 555\text{ nm}$. The emission peak of Fe_3O_4 previously reported was identified near 560 nm ²⁸. No shift in maximum wavelengths was found which demonstrates the perseverance of magnetite after stabilization with citrate.

XRD analysis

X-ray diffractograms of SPION and SPION-C show crystalline peaks representing magnetite. The 2θ positions of 18.35° , 30.26° , 35.56° , 43.31° , 53.74° , 57.30° , and 62.74° were for SPION and 18.21° , 30.07° , 35.34° , 43.07° , 53.31° , 56.83° , 62.41° for SPION-C confirming hkl values (111), (220), (311), (400), (422), (511), and (440)

Table 5. Stability of SPION-C

Storage	Size ^I ± SD ^{II} (nm)	PDI ± SD ^{II}	ζ potential ± SD ^{II} (mV)
Initial	25.94 ± 2	0.312 ± 0.09	-50.8 ± 3.9
Week 3	19.82 ± 7	0.339 ± 0.03	-42.2 ± 4.2
Week 10	21.29 ± 6	0.306 ± 0.01	-41.3 ± 2.3
Week 30	23.98 ± 2	0.276 ± 0.08	-39.5 ± 1.6
Range	11.95 – 28.64 nm	0.212 – 0.372	-37.8 – -54.8

^ISize distribution by number

^{II}SD standard deviation (n=3)

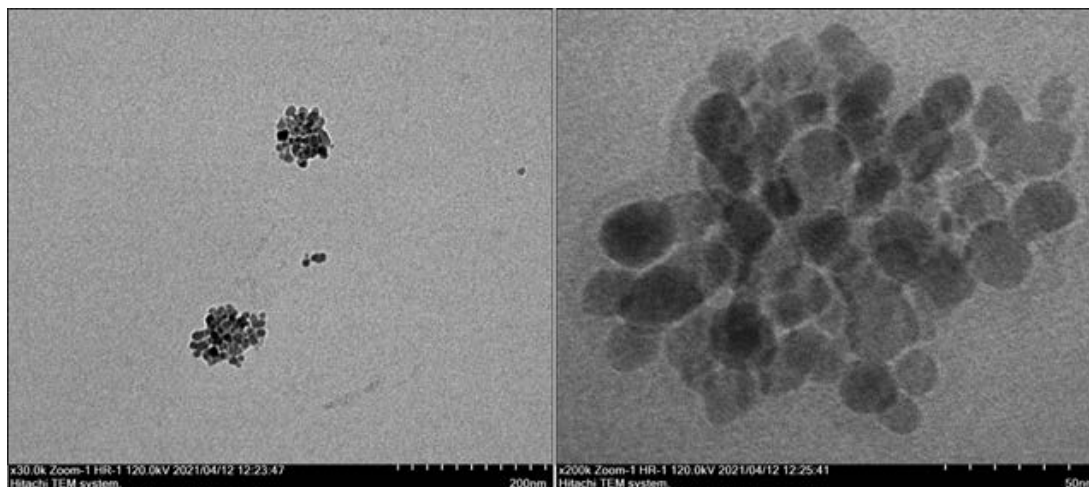


Fig. 5. TEM images of SPION-C magnified x30000 (left) and x200000 (right)

(ICSD 98-015-8742). Intensity weakening of peaks resembling magnetite is due to the citrate coating on the surface²⁹. Our diffractograms show no (210), (300), (213), or (110) peaks known to indicate the presence of maghemite³⁰⁻³². Nonetheless, the oxidized phase of magnetite is hard to distinguish using XRD owing to the similarity of lattice type and constant²⁴. The magnetite phase of SPION was found to have a cubic crystal structure with an Fd-3m space group, and a cubic cell lattice parameter of 8.37 Å, in accordance with reported studies. Furthermore, citrate stabilization proved to decrease the crystalline size of SPION and SPION-C from 6.03 nm to 2.79 nm. This can also be supported by broader peaks in SPION-C indicating the decrease in crystalline size^{9,33}.

Morphological analysis

The morphology of SPION-C is almost spherical shaped (Fig. 6), and that they exist in clusters or agglomerates due to agglomeration during processing. Based on the TEM results, it is visually distinguishable between the SPION core and its citrate coating with particle sizes below 20 nm. This critical size provides the mean for SPION-C to possess superparamagnetic properties. When compared results from dynamic light scattering (DLS), a larger particle size compared to TEM results was generated because DLS measures the hydrodynamic diameter and will put into account the solvent layer where the citrate molecules penetrate in the solvent playing a role in the hydration of the SPION-C³⁴. The D_{V10} of SPION-C show that the DLS method was able to detect nanoparticles below 20 nm, though due to the formation of agglomerates during fabrication and the possibility of aggregation of SPION-C in aqueous media, the Z-avg shifted to higher values, whereas TEM facilitates the visualization of the individual core size of each nanoparticle³⁵.

Stability of SPION-C

During storage, the SPION-C produced with the optimized processing condition showed great colloidal stability. The pH of the environment surrounding the nanoparticles will affect its ζ potential and hence determine its colloidal stability^{10,24}. In this study, the use of trisodium citrate dihydrate (TCD) contributed to the end solution of all SPION-C batches having a pH ranging from 6.74 – 7.33 which helped maintain the ζ potential of the nanoparticles. The physical

stability of the nanoparticle was also ensured by size and PDI during the storage period. These results prove that our method has succeeded in creating highly stable citrate stabilized superparamagnetic iron oxide nanoparticles as shown in Table 5.

CONCLUSION

Superparamagnetic iron oxide nanoparticles stabilized by trisodium citrate dihydrate have been produced using the direct co-precipitation method. The optimized processing condition was 9000 rpm stirring speed, accompanied by 1.006 M of stabilizer and stabilizer adsorption at 90°C. Characterization of nanoparticles below 20 nm which is critical for biomedical use, was confirmed by DLS, FTIR, fluorescence spectroscopy, XRD, and TEM. Furthermore, stability of SPION-C during storage had been achieved. The optimized SPION-C can be further conjugated to a carrier or even to the desired therapeutic agent without additional modification.

Funding

This research was funded by Universitas Indonesia, grant number NKB-1467/UN2.RST/HKP.05.00/2020.

Authors' contributions

All authors have contributed according to their duties and responsibilities.

Conflict of interests

No conflict of interests has been declared by all authors.

REFERENCES

1. Unterweger H, Dézsi L, Matuszak J, Janko C, Poettler M, Jordan J, et al. Dextran-coated superparamagnetic iron oxide nanoparticles for magnetic resonance imaging: Evaluation of size-dependent imaging properties, storage stability and safety. *Int. J. Nanomedicine.*, **13**: 1899–1915 (2018).
2. Salunkhe A, Khot V, Patil S. I, Tofail S. A. M, Bauer J and Thorat N. D. MRI Guided magnetochemo-therapy with high-magnetic-moment iron oxide nanoparticles for cancer theranostics. *ACS Appl. Bio Mater.*, **3**: 2305–2313 (2020).
3. Soleymani M, Khalighfar S, Khodayari S, Khodayari H, Kalhori M. R, Hadjighassem M. R, et al. Effects of multiple injections on the efficacy and cytotoxicity of folate-targeted magnetite nanoparticles as theranostic agents for MRI

- detection and magnetic hyperthermia therapy of tumor cells. *Sci. Rep.*, **10**: 1–14 (2020).
4. Liu C. H, Tandon P and Russell L. M. Translational Nanodiagnosics for in vivo cancer detection. In: Miao T, Oldinski RA, Liu G, Chen X, editors. *Nanotheranostics for Cancer Applications.*, (2019).
 5. Yew Y P, Shameli K, Miyake M, Ahmad Khairudin N. B. B, Mohamad S. E. B, Naiki T, et al. Green biosynthesis of superparamagnetic magnetite Fe₃O₄ nanoparticles and biomedical applications in targeted anticancer drug delivery system: A review. *Arab. J. Chem.*, **13**: 2287–2308 (2020).
 6. Kratz F, Senter P and Steinhagen H. Drug Delivery in Oncology. Kratz F, Senter P, Steinhagen H, editors. Germany: Wiley-VCH; (2012).
 7. Mai B. T, Balakrishnan P. B, Barthel M. J, Piccardi F, Niculaea D, Marinaro F, et al. Thermoresponsive iron oxide nanocubes for an effective clinical translation of magnetic hyperthermia and heat-mediated chemotherapy. *ACS Appl. Mater. Interfaces.*, **11**: 5727–5739 (2019).
 8. Soleymani M, Velashjerdi M, Shaterabadi Z and Barati A. One-pot preparation of hyaluronic acid coated iron oxide nanoparticles for magnetic hyperthermia therapy and targeting CD44-overexpressing cancer cells. *Carbohydr. Polym.*, **237** (2020).
 9. Butt F. A and Jafri S. M. M. Effect of nucleating agents and stabilisers on the synthesis of Iron-Oxide Nanoparticles-XRD analysis. *Adv. nano Res.*, **3**: 169–176 (2015).
 10. Na Y, Yang S and Lee S. Evaluation of citrate-coated magnetic nanoparticles as draw solute for forward osmosis. *Desalination.*, **347**: 34–42 (2014).
 11. Reddy L. H, Arias J. L, Nicolas J and Couvreur P. Magnetic nanoparticles: Design and characterization, toxicity and biocompatibility, pharmaceutical and biomedical applications. *Chem. Rev.*, **112**: 5818–5878 (2012).
 12. Petcharoen K and Sirivat A. Synthesis and characterization of magnetite nanoparticles via the chemical co-precipitation method. *Mater. Sci. Eng. B.*, **177**: 421–427 (2012).
 13. Malhotra A, Spieß F, Stegelmeier C, Debbeler C and Lüdtker-Buzug K. Effect of key parameters on synthesis of superparamagnetic nanoparticles (SPIONs). *Curr. Dir. Biomed. Eng.*, **2**: 529–532 (2016).
 14. Li J, Li D, Zhang S, Cui H and Wang C. Analysis of the factors affecting the magnetic characteristics of nano-Fe₃O₄ particles. *Chinese Sci. Bull.*, **56**: 803–81 (2011).
 15. Massart R. Preparation of aqueous magnetic liquids in alkaline and acidic media. *IEEE Trans. Magn.*, **17**: 1247–1248 (1981).
 16. Nosrati H, Adibtabar M, Sharafi A, Danafar H and Hamidreza Kheiri M. PAMAM-modified citric acid-coated magnetic nanoparticles as pH sensitive biocompatible carrier against human breast cancer cells. *Drug Dev. Ind. Pharm.*, **44**: 1377–1384 (2018).
 17. Lesiak B, Rangam N, Jiricek P, Gordeev I, Tóth J, Kövér L, et al. Surface Study of Fe₃O₄ nanoparticles functionalized with biocompatible adsorbed molecules. *Front. Chem.*, **7** (2019).
 18. Stein R, Friedrich B, Mühlberger M, Cebulla N, Schreiber E, Tietze R, et al. Synthesis and characterization of citrate-stabilized gold-coated superparamagnetic iron oxide nanoparticles for biomedical applications. *Molecules.*, **25** (2020).
 19. Rahimnia R, Salehi Z, Ardestani M. S and Doosthoseini H. SPION conjugated curcumin nano-imaging probe: Synthesis and bio-physical evaluation. *Iran. J. Pharm. Res.*, **18**: 183–197 (2019).
 20. Bee A, Massart R and Neveu S. Synthesis of very fine maghemite particles. *J. Magn. Magn. Mater.*, **149**: 6–9 (1995).
 21. Ba³dyga J. Mixing and fluid dynamics effects in particle precipitation processes. *KONA Powder Part. J.*, **33**: 127–149 (2016).
 22. Li L, Mak K. Y, Leung C. W, Chan K. Y, Chan W. K, Zhong W, et al. Effect of synthesis conditions on the properties of citric-acid coated iron oxide nanoparticles. *Microelectron. Eng.*, **110**: 329–334 (2013).
 23. Riddick T. M. Control of colloid stability through zeta potential. Wynnewood, Pa., Livingston; 1968.
 24. Dheyab M. A, Aziz A. A, Jameel M. S, Noqta O. A, Khaniabadi P. M and Mehrdel B. Simple rapid stabilization method through citric acid modification for magnetite nanoparticles. *Sci. Rep.*, 2020; **10**.
 25. Han D-W, Hong S C, Lee J H, Lee J, Kim H Y, Park J Y, et al. Subtle cytotoxicity and genotoxicity differences in superparamagnetic iron oxide nanoparticles coated with various functional groups. *Int. J. Nanomedicine.* **6** (2011).
 26. Wang W, Li Q, Zheng A, Li X, Pan Z, Jiang J, et al. Superparamagnetic iron oxide nanoparticles for full-color photonic materials with tunable properties. *Results Phys.*, **14** (2019).
 27. Saladino G. M, Hamawandi B, Vogt C, Rajarao G. K and Toprak M. S. Click chemical assembly and validation of bio-functionalized

- superparamagnetic hybrid microspheres. *Appl. Nanosci.*, **10**: 1861–1869 (2020).
28. Sadat M. E, Baghbador M. K, Dunn A. W, Wagner H. P, Ewing R. C, Zhang J, et al. Photoluminescence and photothermal effect of Fe₃O₄ nanoparticles for medical imaging and therapy. *Appl. Phys. Lett.*, **105** (2014).
29. Azizi S, Nosrati H and Danafar H. Simple surface functionalization of magnetic nanoparticles with methotrexate conjugated bovine serum albumin as a biocompatible drug delivery vehicle. *Appl. Organomet. Chem.*, **34**: 1–9 (2020).
30. Namanga J, Foba J, Ndinteh D. T, Yufanyi D. M and Krause R. W. M. Synthesis and Magnetic Properties of a superparamagnetic nanocomposite “Pectin-Magnetite Nanocomposite”. *J. Nanomater.*, 2013: 1–8 (2013).
31. Mousavi S-D, Maghsoodi F, Panahandeh F, Yazdian-Robati R, Reisi-Vanani A and Tafaghodi M. Doxorubicin delivery via magnetic nanomicelles comprising from reduction-responsive poly(ethylene glycol) b poly(ε-caprolactone) (PEG-SS-PCL) and loaded with superparamagnetic iron oxide (SPIO) nanoparticles: Preparation, characterization and simulation. *Mater. Sci. Eng. C.*, **92**: 631–643 (2018).
32. Kayal S and Ramanujan R. V. Doxorubicin loaded PVA coated iron oxide nanoparticles for targeted drug delivery. *Mater. Sci. Eng. C.*, **30**: 484–490 (2010).
33. Favela-Camacho S. E, Pérez-Robles J. F, García-Casillas P. E and Godinez-García A. Stability of magnetite nanoparticles with different coatings in a simulated blood plasma. *J. Nanoparticle Res.*, **18** (2016).
34. Rahman O. U, Mohapatra S. C and Ahmad S. Fe₃O₄ inverse spinal super paramagnetic nanoparticles. *Mater. Chem. Phys.*, **132**: 196–202 (2012).
35. Montaseri H, Alipour S and Vakilinezhad M. Development, evaluation and optimization of superparamagnetite nanoparticles prepared by co-precipitation method. *Res. Pharm. Sci.*, **12**.